Dimensionality of interstitial cluster motion in bcc-Fe

D. A. Terentyev,[1,2,*] L. Malerba,[1] and M. Hou[2]
[1]*SCK•CEN, the Belgian Nuclear Research Centre—Boeretang 200, B-2400 Mol, Belgium*
[2]*Physique des Solides Irradiés et des Nanostructures CP234, Université Libre de Bruxelles, Bd du Triomphe, B-1050 Brussels, Belgium*
(Received 8 May 2006; revised manuscript received 22 January 2007; published 14 March 2007)

We study self-interstitial cluster migration properties, such as dimensionality of the motion and activation energy barrier, as functions of the cluster size, by means of molecular-dynamics simulations in bcc-Fe. The atomic interactions are described using a recently proposed potential, fitted to reproduce self-interstitial atom (SIA) configuration energies in close agreement with the results of *ab initio* calculations. We show that this potential provides a dynamic migration energy for the single SIA in agreement with the experimental value. We also show that, in the case of clusters formed by up to five SIAs, the migration energy decreases with increasing cluster size, but remains higher than previously believed. This is the consequence of the change of the migration mechanism of these small clusters from purely three dimensional (3D) to preferentially one dimensional (1D) and of the fact that these clusters take different configurations during migration, including anomalous ones. While the concept of fast 1D diffusion of large SIA clusters remains valid, the obtained results suggest a revision of both the rapidity and the dimensionality of the motion of small interstitial clusters.

DOI: 10.1103/PhysRevB.75.104108 PACS number(s): 61.72.Ji, 71.15.Pd

I. INTRODUCTION

The mobility of self-interstitial atoms (SIA) and SIA clusters is one of the most important parameters determining the microstructure evolution in irradiated metals. In particular, the kinetics and the reaction cross sections depend crucially on the dimensionality of the motion of defects involved.[1–4] Thus a precise knowledge of the diffusion coefficient and mechanisms (one- vs three-dimensional motion) of these defects as functions of defect size is a fundamental prerequisite for any model intended to describe radiation-induced microstructure evolution.[5–9] The quantitative reliability of the model will strictly depend on the accuracy to which the physical mechanisms of defect migration at the atomic level are understood and on how the consequent parameters governing them are transferred into the model.

According to the atomic-level simulation studies in α-Fe existing to date,[10–21] the most energetically favorable configurations of SIA clusters are collections of $\langle 111\rangle$ crowdions, describable as $\frac{1}{2}\langle 111\rangle$ dislocation loops above a certain size,[14–16,18–21] which are also known to be spontaneously formed in displacement cascade simulations.[15,22–29] Under special conditions collections of $\langle 100\rangle$ dumbbells, describable as $\langle 100\rangle$ loops, can also be stabilized,[16,17,21] but these have never been reported to nucleate spontaneously in displacement cascade simulations in α-Fe to our knowledge. A large body of literature devoted to the study of the $\langle 111\rangle$ SIA clusters in α-Fe (Refs. 10–21) showed that these defects move in one dimension by fast glide, with occasional changes of glide direction [mixed one-dimensional (1D) to 3D migration] in the case of small SIA clusters, formed by two or three SIAs. The activation energy for 1D glide of SIA clusters is in all cases on the order of a few tens of meV, and this high mobility is surprisingly observed even in loops containing as many as 91 SIAs.[16,17,19–21] Although such a low value may induce us to question that SIA cluster migration is a thermally activated process, in most available studies this assumption has been made and proved to be acceptable by the consistency of the results thereby obtained, so we shall retain it. Additional discussions on this subject can be found in Ref. 21.

All of these studies were performed using empirical potentials (EPs) that did not embody the information on SIAs in α-Fe coming from density-functional theory (DFT) calculations.[30–32] These calculations suggest that the $\langle 110\rangle$ dumbbell (the most stable configuration according to experiments[33–35]) has lower formation energy than the $\langle 111\rangle$ crowdion by 0.7 eV, which is significantly different from the picture hitherto provided by most EPs. The previously developed EPs either predict wrongly the $\langle 111\rangle$ crowdion to be the most stable configuration,[22,23,36–38] or provide too small energy difference between $\langle 111\rangle$ and $\langle 110\rangle$ configurations[12,37,23,39–43] (less than 0.3 eV). Owing to this deficiency, the EPs hitherto used provide a low-energy barrier for the $\langle 110\rangle$ dumbbell to reorient itself to the $\langle 111\rangle$ configuration, so that the single SIA is found to migrate one-dimensionally by gliding along the close-packed $\langle 111\rangle$ direction. In this picture, the bottleneck for migration is the reorientation to the $\langle 111\rangle$ configuration, which is assumed to largely determine the overall migration energy. This was indeed the commonly accepted idea,[12,13,15] which was even found to agree with resistivity recovery studies in α-Fe,[19,44] despite the fact that these suggested a migration energy of 0.30 ± 0.03 eV (Refs. 33 and 45–48) for the single SIA, higher than the one provided by the EPs.

In contrast, DFT calculations have shown that the energy barrier for the reorientation from $\langle 110\rangle$ to $\langle 111\rangle$ is about 0.7 eV and therefore its probability is totally negligible at most temperatures. A migration mechanism based on the rigid rotation and translation of the $\langle 110\rangle$ dumbbell, as proposed by Johnson more than 40 years ago,[39] becomes thus the most favored one, as shown by recent DFT studies of the SIA migration in α-Fe, indeed suggest Johnson's mechanism to be the most favorable one, providing a migration energy of 0.34 eV (Ref. 31) (the two alternative migration mechanisms are depicted in Fig. 1). This fact imposes a revision of the previous understanding concerning SIA cluster motion in

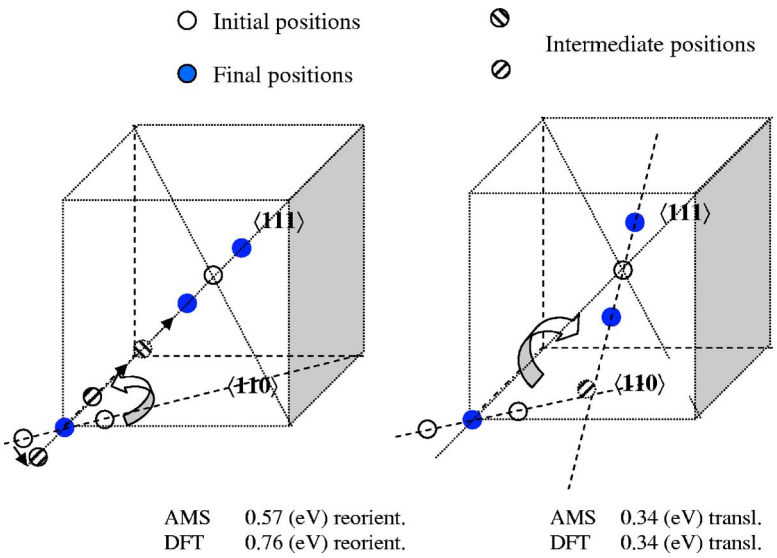

FIG. 1. (Color online) The two jump mechanisms proposed in the literature for SIA migration in α-Fe: (left) reorientation to $\langle 111\rangle$ and crowdion glide along this direction (Refs. 12, 15, 19, and 51); (right) Johnson's mechanism, characterized by translation with change of $\langle 110\rangle$ direction (Ref. 39). Empty and filled spheres represent, respectively, initial and final positions; striped spheres denote intermediate positions. Below the figure the statically calculated barriers for each key process (big arrow) are given according to the present work [AMS potential, (Ref. 50)] and compared to the corresponding values from DFT calculations (Refs. 31 and 32).

α-Fe coming from molecular-dynamics (MD) simulations, because clearly the EPs used for those studies cannot reflect the DFT results. Recently, the configuration of small SIA clusters and the migration barriers for both single SIA and small SIA clusters have been studied statically using DFT methods[31,32] and compared with the predictions of a many-body interatomic potential (potential number 2 in Ref. 49) fitted to reproduce, as closely as possible, the DFT energies of the different SIA configurations. That static study shows that the mentioned potential reproduces indeed fairly well the DFT predictions also for clusters up to five SIAs.

In the present work, a more recent, modified version of the same interatomic potential,[50] henceforth denoted as AMS (from the initials of the first three authors), which predicts an energy difference between $\langle 111\rangle$ and $\langle 110\rangle$ single SIA configurations of about 0.5 eV, is used to study dynamically the migration of the SIA and SIA clusters of different sizes in α-Fe. Dynamic studies of defect migration mechanisms are to be preferred to static studies because no *a priori* choice of the actual migration path is made in them and the influence of temperature, which may activate mechanisms inaccessible at low temperature, is spontaneously allowed for.[51] We show that, using this potential, while the picture for the mobility of SIA clusters of large enough sizes (above five SIAs) remains virtually unchanged, for small clusters the fast 1D motion description becomes a subject of revision. In particular, the SIA appears to follow a largely 3D path, following the jump mechanism proposed by Johnson, with a dynamic migration energy fully consistent with the experimental (and static DFT) value. The data are presented in terms of jump frequencies vs temperature, specifying activation energies and pre-factors as functions of size. Shortcomings encountered in specific cases when applying established methodologies for the computational study of SIA cluster mobility in metals by MD are pointed out and briefly discussed. In Sec. II the methodology used in the present study is outlined and in Sec. III our results are presented. In Sec. IV we discuss the reliability of our results vs DFT calculations and their possible impact on the description of the microstructure evolution in this metal under irradiation and during annealing. The main conclusions are summarized in Sec. V.

II. CALCULATION METHOD

A. MD simulations and atomic coordinate analysis

The general MD simulation scheme for atomic-scale modeling of the diffusion of point defects and their clusters, including the specific features related to 1D transport, has been taken from Osetsky and co-workers.[16,17,21,51] Single SIA and SIA cluster motion was therefore studied using classical MD in the microcanonical (NVE) ensemble, after equilibration to a given temperature. All calculations were done with the MD code DYMOKA.[22] Cubic crystallites equilibrated at zero pressure containing up to 54 000 atoms with periodic boundary conditions were employed. The diffusion of single SIA and SIA clusters containing from 2 to 37 SIAs was simulated in the temperature region from 400 to 1000 K. SIAs were identified as two atoms in the same Wigner-Seitz cell. The SIA and SIA cluster (center of mass) positions were tracked, together with their corresponding orientation, so that a full picture of the defect motion could be produced. In order to have equal statistical meaning for simulations at all temperatures, the migration process was followed for an increasing physical time (10–20 ns) with decreasing temperature, in such a way that a large enough number of defect jumps (between 10^2 and 10^4, 10^3 on average) was performed in all considered cases for a given type of defect.

The position of the single SIA was monitored every 10 fs at the lowest temperature and every 2 fs at the highest temperature. From its trajectory and by counting the number of jumps, both its jump frequency and its diffusion coefficient could be deduced, as explained in Sec. II B (the jump distance equals the first nearest-neighbor distance in the bcc-Fe lattice, coincident with the Burgers vector: $|b|=a_0\sqrt{3/2}$ $\cong 2.48$ Å, a_0=lattice parameter$\cong 2.87$ Å). Distinguishing between different possible jump mechanisms required the orientation of the self-interstitial configuration to be checked after each jump ($\langle 110\rangle$ or a $\langle 111\rangle$), in order to establish what angle the new direction formed with the previous one. Knowing the coordinates of the two atoms in the dumbbell, the axis joining each of them to the central lattice site is easily computed. If both atoms lie within the solid angle

$d\Omega = \frac{\varepsilon^2}{4\pi \cdot \Delta Z}$, where ΔZ is the projection of the coordinate of one of the atoms (with origin in the lattice site) on the considered axis and ε is a calibrated small length (chosen to be 0.12 Å after testing in the case of the single SIA at 600 K), then the SIA has a defined orientation that can be recognized and recorded. Otherwise the SIA is classified as "without defined orientation," a situation that typically corresponds to the moment of the reorientation.

The position of the SIA clusters was defined by the coordinates of the center of mass of the dumbbells or crowdions contained in them ("center of mass of the cluster," henceforth CMC). The positions of the centers of each SIA in the cluster were recorded every 5 fs, thereby obtaining the corresponding trajectories. Each time it was also verified that the cluster had not dissociated, using a nearest-neighbor distance criterion (the actual distance varied depending on the size of the cluster; for large clusters it corresponded to $3b$ along the $\langle 111 \rangle$ direction, i.e., to the tenth nearest-neighbor distance): if dissociation was detected, the simulation was stopped. However, in the present work no cluster dissociation was ever observed, even at the highest temperatures. The number of jumps of the CMC was counted by taking the jump distance equal to b, as in the case of the single SIA. This enabled the corresponding jump frequencies, correlation factors, and diffusion coefficients to be deduced, as described in the following section (see also Refs. 14, 21, and 51). In order to study the cluster orientation, the following criteria have been used: each time the CMC has been determined, the orientation of each dumbbell or crowdion belonging to the cluster has been identified. If all individual defects forming the cluster had the same orientation, then the orientation of the cluster was defined to be the same as the orientation of its individual defects. Otherwise, the cluster was assigned no defined orientation. By tracking the change in the cluster orientation in time it was broadly possible to estimate the number of reorientations of the cluster.

B. Diffusion coefficients

The diffusion coefficient of a cluster of defects of size N, $D_N(T)$, can be obtained from atomistic simulations using the well-known Einstein equation (see, e.g., Ref. 52):

$$D_N(T) = \frac{\overline{R_N^2}(T)}{2nt_{sim}}, \tag{1}$$

where $\overline{R_N^2}$ is the mean-square displacement (MSD) of the migrating defects and is a function of temperature, n is the dimensionality of the motion (1)–(3), and t_{sim} is the simulation time. After repeating the calculation for different temperatures, the $D_N(T)$ curve can be produced by interpolating the different points with the Arrhenius expression typical of any thermally activated process, i.e.,

$$D_N(T) = D_{0,N} e^{-E_m^n / k_B T}. \tag{2}$$

Here k_B is Boltzmann's constant, while the migration energy E_m^N and the prefactor $D_{0,N}$ are the free parameters of the interpolation, whose values are obtained from the linear regression (logarithm vs $1/k_BT$) on the collected points.

In order for Eq. (1) to define unambiguously a diffusion coefficient, independently of the choice of t_{sim}, $\overline{R_N^2}$ should increase linearly with time. This condition is easily fulfilled if the average is taken on a large amount of diffusing defects for long observation times. However, in MD simulations the time frame is limited and, in order to follow correctly the trajectory of the type of defect to be studied, only one defect at a time can be introduced in the crystallite. A way to partially circumvent the problem consists of decomposing the trajectory of the only defect introduced in the system into a set of K shorter, independent segments, each corresponding to a fraction of the simulated time, $\tau_K = t_{sim}/K$, as first applied by Guinan *et al.*[53] This technique of data analysis, called here the *independent interval method* (IIM), has been widely used in the past to study SIA and SIA cluster diffusion.[14,15,18,20,51,53] With the IIM the displacements of a defect of size N in each of the K intervals i, $R_{N,i}$, are traced and the average of their square is taken, thereby obtaining the defect diffusion coefficient at a certain temperature, $D_N(T)$:

$$D_N(T) = \frac{1}{K} \sum_{i=1}^{K} \frac{R_{N,i}^2}{2n\tau_K}(T). \tag{3}$$

The choice of τ_K is delicate. It should be long enough to include all local correlations of defect motion, i.e., should correspond to long enough trajectories. On the other hand, it cannot be very long in practice, for a given t_{sim}, because the error committed is statistically proportional to $\sqrt{K}$. The problem is particularly serious when the defect motion is mixed 1D and 3D. Then two choices are *a priori* possible. Either the treatment is applied for 1D segments only, i.e., between directional changes, with $n=1$, thereby determining the 1D diffusion coefficient, or the three-dimensional case is considered, with $n=3$, but in this case one must make sure that $\tau_K \gg \tau_{cgd}$ (where $1/\tau_{cgd}$ is the rate of directional changes, particularly changes of 1D glide direction). Note that the first approach is only applicable if it is indeed possible to describe the motion of the defect as a sequence of 1D stretches along different directions: this situation may not always be realized, as will be seen in the following section. In the present work, the choice of τ_K was made by looking at the dependence of $D_N(T)$ on it. As shown, e.g., in Ref. 48, the value of $D_N(T)$ decreases for growing τ_K and finally stabilizes to a more or less constant value, thereby becoming only weakly dependent on τ_K: the value for $D_N(T)$ was then chosen to be the one in this "plateau" corresponding to the smallest τ_K, i.e., to the smallest error bar, which was generally around 10%. The actual value of τ_K was of course different in each case, but the range was 20–250 ps.

If the defect motion can be described in terms of discrete jumps between equivalent equilibrium positions, occurring at a known average rate, and the jump distance Δ is constant, as is the case for both single SIAs and SIA clusters (with $\Delta = b$), then Eq. (1) can be rewritten for a defect of size N at a given temperature T as[14,21,51]

$$D_N^*(T) = f_C(T,N)\frac{\nu_N^j(T)\Delta^2}{2n}. \quad (4)$$

Here, ν_N^j is the jump frequency and f_C is the correlation factor. Note that all the way through we will assume that the jump distance is fixed and equal to the first nearest-neighbor distance in the bcc crystal. The jump frequency ν_N^j can then be measured from the simulation by monitoring the successive center-of-mass positions of the defect and taking the average of the inverse of the time between jumps, which provides directly the average frequency. The correlation factor is generally temperature and defect size dependent and its complete expression is (see, e.g., Ref. 52)

$$f_C = 1 + \lim_{n\to\infty}\left(\frac{2}{n}\left\langle \sum_{i=1}^{n-1}\sum_{j>i}^{n-1}\cos\theta_{i,j}\right\rangle\right), \quad (5)$$

where $\theta_{i,j}$ is the angle between the directions of jumps i and j. If the defect follows a completely isotropic random walk and the number of jumps is sufficiently large, i.e., in the case of a fully random 3D diffusion, it can be easily demonstrated that $f_C \to 1$ and can hence be dropped in Eq. (4). When the motion is strictly 1D, on the other hand, the correlation factor has a straightforward expression:[54]

$$f_C^{1D} = \frac{N_{for}}{N_{back}}, \quad (6)$$

i.e., simply the ratio between the number of forward (N_{for}) and backward (N_{back}) jumps (compared to the previous jump), which is readily deduced from the simulation. In cases of fully 1D motion Eq. (4) can therefore be conveniently used, with $n=1$, for the determination of the 1D diffusion coefficient of the migrating defect. This method will be henceforth denoted as *jump length method* (JLM).

The application of Eq. (4) requires the evaluation of the single-jump frequency from the simulation. Its temperature dependence obeys an Arrhenius law as well:

$$\nu_N^j(T) = \nu_{0,N}^j e^{-E_m^{N*}/k_BT}, \quad (7)$$

where $\nu_{0,N}^j$ is the defect jump attempt frequency. As discussed in Ref. 51, the effective defect migration energies obtained for the same defect from the diffusion coefficient [Eq. (2)], E_m^N, and from the jump frequency [Eq. (7)], E_m^N*, can be different. One of the reasons for this is exactly the temperature dependence of the correlation factor [Eq. (6)]. This implies that, in general, it is not possible to obtain the jump frequency, given the diffusion coefficient, without knowing the correlation factor. Nonetheless, it is possible to assess the jump frequency *prefactor* that appears in Eq. (7), given, e.g., the diffusion coefficient estimated using the IIM, even without precise knowledge of the correlation factor. By combining Eqs. (2), (4), and (7) one obtains indeed

$$\nu_{0,N}^j = \frac{2nD_{0,N}^{d,IIM}}{\Delta^2}\frac{e^{-(E_m^{N,IIM}-E_m^{N*})/k_BT}}{f_C(T,N)} \approx \frac{2nD_{0,N}^{d,IIM}}{\Delta^2}. \quad (8)$$

Here, the assumption behind the approximate equality between intermediate and right-most term is that the difference between the migration energy obtained from the IIM diffusion coefficient and the migration energy obtained from the corresponding jump frequency comes from the temperature dependence of the correlation factor. The behavior vs temperature of the exponential function in the numerator is thus expected to be the same as the behavior vs temperature of f_c and their ratio is therefore expected to be constant and close to unity. This approximate equation does not add anything to the analysis, but it turns out to be useful in some cases for comparison between defects for which only the diffusion coefficient from the IIM is known.

Finally, if the orientation of the defect is monitored as described in the previous section, it is possible to give an estimate of the size dependent activation energy for reorientation, E_N^r, by producing the Arrhenius plot vs temperature of the frequency of reorientations, ν_N^r, as measured from the simulation:

$$\nu_N^r(T) = \nu_{0,N}^r e^{-E_N^r/k_BT}. \quad (9)$$

It should be noted that all methods considered here to quantify the diffusion properties of SIA defects present shortcomings when it comes to their applications. The IIM is *a priori* a blind method that should work even without any knowledge of the actual defect migration mechanism at the atomic level, but in fact information about the dimensionality of the motion is necessary to choose the simulation time and the length of time intervals to be considered. In some cases obtaining proper statistics and convergence to a unique diffusion coefficient value, independently of the choice of t_{sim} and τ_K, may prove difficult (see discussion in Ref. 51). The JLM inherently obliges to produce more detailed information concerning the migration mechanisms, but it is convenient only for strictly 1D moving defects and is also affected, like the IIM, by simulation time constraints, that may limit its statistical accuracy. Its application to 1D to 3D moving defects is in principle possible, in order to define the 1D diffusion coefficient of a given defect, however, it requires the actual possibility of identifying 1D stretches in the defect trajectory. As will be shown in this work, this is not always true and this fact may lead to some difficulties in deciding which method is the most appropriate and reliable in each particular case and, more importantly, which description is the most adequate to characterize the motion of a given defect in a coarser-grain model that neglects the atomic-level details.

III. RESULTS

A. Stability of single SIA and SIA cluster configurations

Prior to investigating the mobility of interstitial defects, we determined the energy of the most stable configuration in which the studied SIA clusters are found according to the EP used. In order to do that, after equilibration at finite temperature the obtained configurations were frozen by rapidly reducing the temperature to values increasingly close to zero (quenching), with the aid of the MD code. The results, presented in Table I, were obtained in a box of 2000 atoms at constant volume.

As already mentioned, for the single SIA the stablest configuration is the ⟨110⟩ dumbbell, in agreement with both

TABLE I. Statically calculated formation energies of ⟨111⟩ and ⟨110⟩ configurations and corresponding energy differences between the two (total and per SIA) for a number of small clusters, according to (i) the potential used in this work (Ref. 50), (ii) the calculations performed in Ref. 32 using potential number 2 in Ref. 49, and (iii) the DFT calculations performed in Ref. 32. Our calculations were performed at constant volume in boxes of 2000 atoms in order to ensure convergence.

	Energies (eV)											
	$E_f^{\langle 110\rangle}$			$E_f^{\langle 111\rangle}$			$E_{\langle 111\rangle-\langle 110\rangle}$			$E_{\langle 111\rangle-\langle 110\rangle}$ per SIA (eV/SIA)		
Cluster size (no. SIA)	This work AMS[a]	Ref. 32 EP[b]	Ref. 32 DFT	This work AMS[a]	Ref. 32 EP[b]	Ref. 32 DFT	This work AMS[a]	Ref. 32 EP[b]	Ref. 32 DFT	This work AMS[a]	Ref. 32 EP[b]	Ref. 32 DFT
2	6.23	6.21	6.68	6.76	6.74	7.43	0.53	0.53	0.75	0.27	0.27	0.38
3	8.87[c]	8.79[c]	9.49[c]	9.36	9.37	10.01	0.49	0.58	0.52	0.16	0.19	0.17
4	11.05	11.05	11.66	11.22	11.36	11.77	0.17	0.31	0.11	0.04	0.08	0.02
5	13.42	13.25	14.18	13.49	13.36	13.88	0.07	0.11	−0.30	0.01	0.02	−0.06
7	17.68	//	//	16.80	//	//	−1.08	//	//	−0.15	//	//

[a]AMS=empirical potential from Ref. 50 used in present work.
[b]EP=empirical potential from Ref. 49.
[c]EP and DFT predict a slightly different lowest energy configuration.

experiments[33–35] and DFT calculations.[30–32] The formation energy of the ⟨111⟩ crowdion is 0.5 eV higher than that of the ⟨110⟩ dumbbell, which is much closer to DFT results than with most as yet used EPs, as can be seen from Table II.

According to the AMS potential used in this work,[50] di-, tri-, tetra-, and penta-interstitial clusters consist in their stablest configuration of first nearest-neighbor, parallel ⟨110⟩ dumbbells, while a configuration consisting of ⟨111⟩ parallel crowdions was found to be the most stable for seven-SIA clusters. The energy surplus of the ⟨111⟩ configuration for di-, tri-, tetra-, and penta-intestitials decreases with size, as shown in Table I, which qualitatively and quantitatively agrees with static calculations at constant pressure performed in Ref. 32, where potential number 2 from Ref. 49 was used. The agreement is also good with constant pressure DFT static calculations,[32] except in the case of the penta-interstitial that, according to DFT, is already more stable in the ⟨111⟩ configuration. Note that in Table I also the energy difference per SIA is provided. This energy is important because, although the physical mechanism leading to the reorientation of the cluster is not known in detail, it could be a process whereby not all dumbbells rotate at the same time to become crowdions, but rather one by one. In this picture, the energy difference per SIA between the two configurations provides an estimate of the energy required to trigger the transformation.

B. Mobility of single SIA and SIA clusters

The results are presented in three blocks, corresponding to classes of defects that, even within the relatively small range of sizes analysed in this work, exhibit different dynamic behavior from one to another.

1. Defects of class 1

The first class is composed by the single SIA and the di-interstitial, whose migration paths were found to be fully three-dimensional at all temperatures. For both defects the diffusion coefficient could therefore be unambiguously obtained using the IIM [Eq. (3)]. The mechanism of migration is Johnson's (Fig. 1) for both; in the case of the di-interstitial the two dumbbells jump in sequence, one after the other.

TABLE II. Relative stability of SIA configurations according to a number of interatomic potentials. E_f denotes the formation energy of the specified SIA configuration; $E_{\langle 111\rangle-\langle 110\rangle}$ denotes the difference, which gives the relative stability. These potentials are those used to produce the data shown in Fig. 2.

	Energies (eV)		
Potentials	$E_f^{\langle 110\rangle}$	$E_f^{\langle 111\rangle}$	$E_{\langle 111\rangle-\langle 110\rangle}$
Chakarova *et al.* (Ref. 38, 60, and 75)	4.15 (Ref. 75)	4.02 (Ref. 75)	−0.13 (Ref. 75)
Ackland *et al.* (1997) (Ref. 42)	4.87	5.00	0.13
Simonelli *et al.* (Ref. 43)	4.23	4.53	0.30
Johnson & Oh (Ref. 15, 59, and 63)	4.34 (Ref. 41)	4.71 (Ref. 41)	0.37 (Ref. 41)
This work [AMS (Ref. 50)]	3.52	4.01	0.49
DFT (Ref. 30)	3.41	4.11	0.70

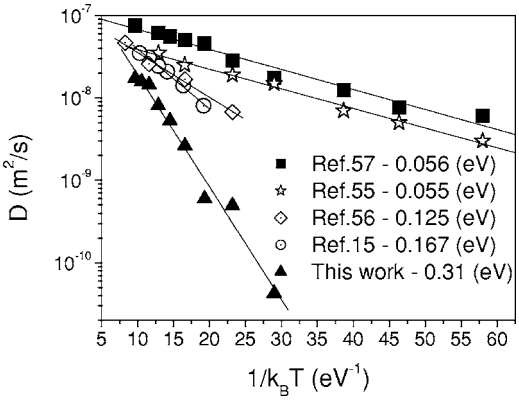

FIG. 2. Comparison of the single SIA diffusion coefficients obtained by MD in this work using the AMS potential with results taken from the literature obtained with a number of older potentials for α-Fe, namely, Chakarova *et al.* (Refs. 38, 60, and 75) from Ref. 57, Ackland *et al.* (1997) (Ref. 42) from Ref. 55, Johnson and Oh (Refs. 59 and 63) from Ref. 15, and Simonelli *et al.* (Ref. 43) from Ref. 56. The solid lines are linear Arrhenius fits. Only AMS provides an effective migration energy comparable with the experimental value.

The diffusion coefficient of the single SIA vs temperature calculated with different potentials using the IIM is given in Fig. 2 (see Table III for the corresponding diffusion coefficient and jump frequency prefactors). The results for the AMS potential[50] were produced in this work, while the other results were taken from the literature.[15,55–57] Only the data points obtained using the AMS potential[50] provide an effective migration energy close to the experimental result[33,45–48] (0.30±0.03 eV), whereas other results are far from it. The reason for these different predictions clearly resides in the different relative stability that each potential assigns to the ⟨110⟩ dumbbell vs the ⟨111⟩ crowdion, as summarized in Table II, and the consequently different time that the SIA spends in the two configurations, which gives a different weight to the two possible mechanisms depicted in Fig. 1. The effective, global migration energy is the weighted average of the migration energies associated to the two competing mechanisms (*a priori* other mechanisms specific of a given potential may also appear). By analyzing the recorded orientations of the SIA according to AMS, it has been seen that this defect is hardly ever found in the crowdion configuration at all studied temperatures. Thus the effective migration energy is essentially decided by the energy barrier associated with Johnson's mechanism (Fig. 1). The slightly higher value obtained statically in this work (Fig. 1) is likely to be due to the approximate procedure used in such a calculation to find the saddle point: more accurate static calculations performed with the same potential provide 0.304 eV,[58] in line with the present dynamic calculations. At the other extreme, with Chakarova *et al.* potential the SIA is always in a crowdion configuration and the only reason for having an effective migration energy slightly higher than the pure glide energy is the fact that it undergoes changes of glide direction.[57] The Ackland *et al.* (1997) potential[42] provides low stability of the ⟨110⟩ dumbbell relative to the ⟨111⟩ crowdion (see Table II), therefore the reorientation to crowdion often occurs and the effective migration energy is mainly defined by the energy for crowdion glide, like in the Chakarova *et al.* potential case. On the other hand, Johnson and Oh[15,59,60] and Simonelli *et al.*[43] potentials predict a higher relative stability of the dumbbell vs the crowdion (see Table II), although not as large as AMS, therefore they provide intermediate results between the mentioned extreme cases.

TABLE III. Results of the application of the IIM for clusters formed by up to five SIAs. The reported jump frequency prefactor has been obtained from Eq. (8) and is therefore exact only in the case of single- and di-interstitial.

Size (N)	Type of motion	$D_{0,N}$ (m^2/s)	$\nu^j_{0,N}$ (10^{12} s^{-1})	E^N_m (eV)
1	3D	4.42×10^{-7}	43	0.31
2	3D	2.43×10^{-6}	237	0.33
3	3D→1D–3D	3.35×10^{-8}	*3.3*	0.14
4	1D–3D	3.11×10^{-8}	*3.0*	0.16
5	1D–3D→1D	4.30×10^{-9}	*0.42*	0.07

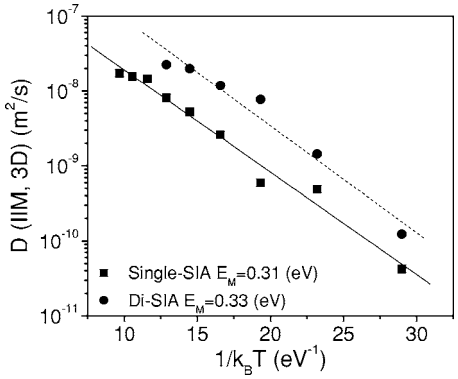

FIG. 3. Diffusion coefficient for the single- and di-interstitial as calculated using the IIM. Both defects move following a completely three-dimensional random path. The migration energies corresponding to the slope of the linear Arrhenius fit (straight lines) are also indicated (for prefactors, see Table III).

Figure 3 shows the diffusion coefficient vs temperature for the di-interstitial obtained in the present study employing the IIM (see Table III for the corresponding diffusion coefficient and jump frequency prefactors). Data points for the single SIA are also included for direct comparison. Both defects have a very similar migration energy (0.33 and 0.31 eV), consistently with the similar jump mechanism. Also static calculations with a potential very close to the one used here (potential number 2 in Ref. 49) have shown that single- and di-interstitial have similar migration energies.[32] However, DFT static calculations gave for the di-interstitial a higher migration energy, namely 0.42 eV.[32] The reason for this discrepancy are not clear and will be discussed in Sec. IV. Note that Fig. 3 reveals also that the prefactor to the diffusion coefficient of the di-interstitial is larger than that of the single SIA by about a factor 5 (see also Table III), denoting somewhat faster diffusion of the former. It is difficult, however, to make any statement about the consistency of this effect with either experimental evidence or DFT studies.

TABLE IV. Frequency of reorientation in terms of prefactor and activation energy for clusters up to size 4.

Size (N)	Type of reorientation	$\nu^r_{0,N}$ (10^{12} s^{-1})	E^r_N (eV)
1	⟨110⟩→⟨111⟩	11	0.69
2	⟨110⟩→⟨110⟩	157	0.28
3	⟨110⟩→⟨111⟩	0.37	0.041
4	⟨110⟩→⟨111⟩	8.01×10^{-2}	0.044

The barrier for reorientation for both defects of this class have also been estimated dynamically from the reorientation frequency, as detected using the algorithm described in Sec. II A. The corresponding prefactors and energy barriers are given in Table IV. The single SIA was observed to reorient from the ⟨110⟩ to the ⟨111⟩ SIA configuration at high temperature, with an effective reorientation energy of 0.69 eV, somewhat higher than in the approximate static calculation. The di-interstitial has never been seen to glide along the close-packed ⟨111⟩ direction, not even at high temperature, consistently with the high-energy difference between its ⟨111⟩ and ⟨110⟩ configurations (see Table I). Thus the study was limited to the reorientations interpreted as changes of ⟨110⟩ direction, corresponding in fact to a diffusion jump. The reorientation energy was found to be 0.28 eV, a value that, considering that it has been obtained from a different type of analysis and allowing for the error associated to the regression, must be considered essentially coincident with the migration energy value, 0.33 eV.

2. Defects of class 2

The second class is composed by tri-, tetra-, and penta-interstitial. In this class a transition between fully 3D and preferably 1D motion occurs with growing size within the MD time frame. In practice, each cluster behaves differently. The tri-interstitial exhibits fully 3D motion below 600 K, but above this temperature the cluster was found to glide in the ⟨111⟩ configuration. The tetra-interstitial displays a clearly visible and well-defined 1D–3D motion at all temperatures, with long 1D-glide stretches, during which the cluster has most of the time a ⟨111⟩ configuration, interrupted by changes of glide direction by transformation into ⟨110⟩ configurations. The penta-interstitial moves preferentially by gliding along the ⟨111⟩ direction, at all temperatures, with very sporadic changes of glide direction, detectable only at high temperature in the MD time frame (about 12 times in 20 ns at 900 and 1000 K, i.e., 500 jumps). Only at low temperature were penta-interstitials observed to turn from time to time into a ⟨110⟩ configuration, without change of glide direction.

Figure 4 shows the diffusion coefficients vs temperature obtained with the IIM for this class of defects. For convenience, also single- and di-interstitial data points are included. The corresponding IIM migration energies and prefactors are detailed in Table III. Clearly, the clusters of this class are faster diffusers than the defects of the class 1, in a relatively large range of low temperatures. The tri-interstitial is found to migrate with an effective energy of 0.14 eV, very close to the migration energy of the tetra-interstitial, while for the penta-interstitial the effective migration energy was found to be as low as 0.07 eV, suggesting the onset of 1D glide. The migration energies of defects corresponding to this class are therefore rather low, but not as low as reported in previous works,[15–17,19–21] where clusters of the same size where found to glide athermally along the ⟨111⟩ direction only.

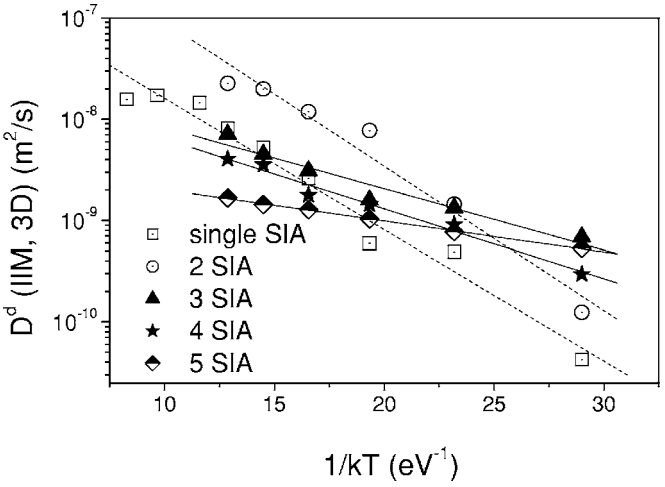

FIG. 4. Diffusion coefficient of defects of class 2, as calculated using the IIM. The data for the single- and di-interstitial are also included for direct comparison. For the corresponding migration energies and prefactors, see Table III. The dashed and solid lines are linear Arrhenius fits to the data points for, respectively, defects of class 1 and 2.

In the case of the tri- and tetra-interstitial, the frequency of reorientation between ⟨110⟩ and ⟨111⟩ directions has been determined according to the analysis described in Sec. II A and is presented in Fig. 5. It can be seen that, within the relatively large scatter of the data points, these clusters reorient themselves almost athermally, with surprisingly low effective activation energies (few tens of meV). In the case of the tetra-interstitial each reorientation to the ⟨110⟩ configuration corresponds to a subsequent change of ⟨111⟩ glide direction, while this is not necessarily the case for the tri-interstitial.

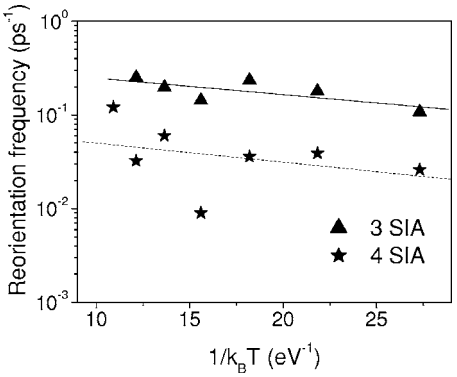

FIG. 5. Frequency of reorientation (from ⟨110⟩ to ⟨111⟩) of tri- and tetra-interstitial. For the corresponding activation energies and prefactors, see Table IV. The lines are linear Arrhenius fits.

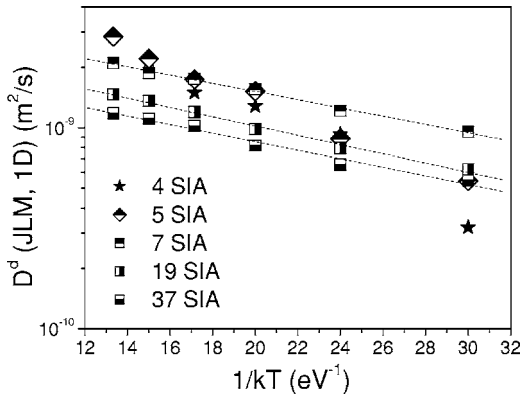

FIG. 6. 1D diffusion coefficient for the SIA clusters of class 3 (size 7, 19, and 37), as calculated using the JLM. These defects move exclusively along a one-dimensional paths within the MD time frame. The data for some of the clusters of class 2 are included for comparison. The lines are linear Arrhenius fits. For the corresponding migration energies and prefactors, see Table V.

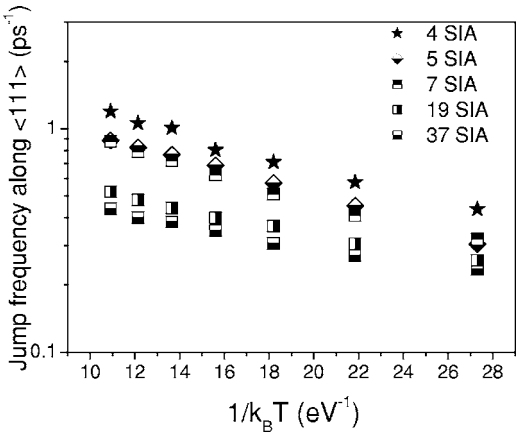

FIG. 7. Jump frequency along ⟨111⟩ directions for SIA clusters of class 2 and 3. For the corresponding migration energies and prefactors, see Table V.

In the case of tetra- and penta-interstitial, 1D-glide stretches along ⟨111⟩ directions can be unambiguously identified and isolated, providing the possibility of estimating their 1D diffusion coefficient using the JLM. The relevant data are plotted in Fig. 6 (diffusion coefficient) and Fig. 7 (jump frequency). The corresponding migration energies and prefactors are given in Table V, together with data for larger clusters to be discussed in the next section. Figure 6 and Table V reveal that the 1D diffusion coefficients of tetra- and penta-interstitials are close to each other, but different from those of larger clusters: the corresponding 1D migration energy is higher, and therefore the mobility lower, than, e.g., for a seven-SIA cluster, in a fairly large range of low temperatures. Nonetheless, when analyzed in terms of 1D jump frequency (Fig. 7), tetra- and penta-interstitials behave exactly as larger clusters, though with a somewhat higher migration energy. The difference between the migration energies for these two clusters of class 2 is related to the temperature dependence of the correlation factor, as shown in Fig. 8. The correlation factor related to the clusters of class 2 increases with temperature, while it decreases in other cases.

Another unexpected feature, which was found to be specific for this class of clusters, is that all three of them have been seen to take highly symmetric, but anomalous configurations that cannot be classified as either ⟨110⟩ or ⟨111⟩. Tri-, four-, and penta-SIA clusters in these configurations consisted of nonparallel dumbbells and were found to move slower or not at all. The presence of such configurations was detected at relatively high temperatures (above 600 K), suggesting that entropy may stabilize them. In the case of the penta-interstitial, where these configurations have been observed most frequently, they appear to be easily switched to and from during ⟨111⟩ glide, occasionally leading to a change of the glide direction. This fact suggests that the found configurations are energetically almost equivalent to the ⟨111⟩ configurations and contribute to make the migration path followed by the cluster more complicated, thereby increasing the effective migration energy of this cluster when compared to purely gliding ⟨111⟩ clusters. When the tetra-interstitial falls into such a configuration during glide, it stops moving at all (so the simulation was stopped in those cases). The latter observations suggest that, beyond the MD timeframe, the existence of metastable nonparallel configurations may further affect the mobility of SIA clusters, in the sense of reducing it. The relative stability of these configurations and the mechanisms whereby they can transform to the other ones is currently under investigation, as well as their reproducibility with DFT methods.

3. Defects of class 3

The third class of clusters includes all those consisting of more than five SIAs (up to the maximum studied size), which are collections of ⟨111⟩ crowdions in their most stable configuration. In this case, the results obtained with the used

TABLE V. Results of the application of the JLM (1D diffusion coefficient) for clusters from size 4 upward.

Size (N)	Type of motion	$D_{0,N}$ (m^2/s)	E_m^N (eV)	$\nu_{0,N}^j$ (10^{12} s^{-1})	$E_m^{N^*}$ (eV)
4	1D–3D	1.39×10^{-8}	0.12	2.24	0.061
5	1D–3D→1D	9.93×10^{-9}	0.10	1.85	0.065
7	1D	3.90×10^{-9}	0.047	1.68	0.063
19	1D	2.96×10^{-9}	0.053	0.80	0.043
37	1D	2.28×10^{-9}	0.049	0.64	0.038

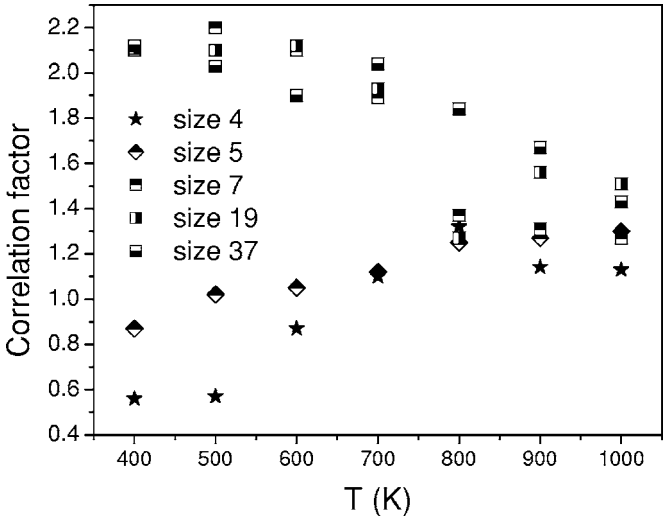

FIG. 8. Correlation factor for SIA clusters of class 2 and 3. Note that this factor decreases with temperature in the case of clusters of class 3, while it increases in the case of clusters of class 2.

EP are in full agreement with those of previous studies with other potentials.[12–15,18–21] As a consequence of their configuration, these clusters glide along the ⟨111⟩ direction of their Burgers vector and cover, at least within the MD time frame, strictly 1D migration paths. For these clusters the use of the JLM was therefore the obvious choice. The main lacking information for these clusters is the corresponding frequency of change of glide direction, whose determination is out of the reach of the MD time frame.

The 1D diffusion coefficients vs temperature for clusters of 7, 19, and 37 SIAs are shown in Fig. 6, together with those of tetra- and penta-interstitial. The corresponding migration energies and prefactors are detailed in Table V and are seen to be only weakly dependent on size and invariably very small (0.04–0.06 eV), while the prefactor decreases with cluster size. Qualitatively similar, though quantitatively slightly different, values of migration energy were obtained from the corresponding jump frequencies, plotted in Fig. 7 (see Table V for energies and prefactors). The difference between the migration energy obtained from the jump frequency $E_m^{N\ *}$ and from the diffusion coefficient E_m^N originates from the temperature and size dependence of the correlation factor. Its somewhat scattered values are shown in Fig. 8 and display for this class of clusters a qualitatively similar trend vs size and temperature when compared to the work of Osetsky *et al.*, where a different potential was used,[21] although the actual values are fairly smaller. The results obtained with the AMS potential for this class of clusters are therefore comparable with previously published ones.[14,16,18–21] In particular, the jump frequency prefactors obtained in the present work can also be interpolated using the law proposed and used by Osetsky *et al.*, $\nu_{0,N}^j = \nu_{0,1}^j / N^S$,[14,16,17,21,51] where S is a fitted exponent that has been theoretically explained to take values between about 0.5 and 1 (Refs. 18, 61, and 62) and $\nu_{0,1}^j$ is interpreted as the jump frequency prefactor for the single SIA (in the crowdion configuration). In Fig. 9 this law is used to interpolate our data from Table IV and to compare them with data from (i) Osetsky *et al.*,[21] obtained using the JLM in MD simulations with their own pair potential,[36] (ii) Marian *et al.*,[20] obtained using the IIM (with $n=1$) in MD simulations with Ackland *et al.* (1997) potential,[42] [original data are transformed in terms of jump frequency prefactor via Eq. (8) for comparison], and (iii) Soneda and de la Rubia,[19] obtained using the IIM (with $n=3$) in MD simulations with the Johnson and Oh potential[15,59,63] [data are also transformed via Eq. (8) for comparison, after multiplying by 3 for full consistency]. It can be seen that the "N^{-S}" law is valid for all data with values of S in the theoretically predicted range,[12,61,62] although the crowdion frequency prefactor depends visibly on the potential and is found to be particularly high according to Ackland *et al.* (1997) potential ($\cong 5\times10^{13}$ s^{-1}), intermediate according to Johnson and Oh ($\cong 1\times10^{13}$ s^{-1}) and lower and essentially coincident with AMS according to the Osetsky potential ($\cong 5\times10^{12}$ s^{-1}).

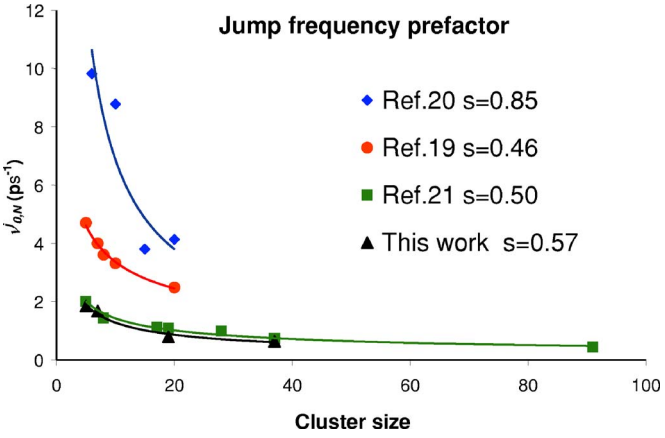

FIG. 9. (Color online) Jump frequency prefactor as a function of cluster size according to the present work compared to similar data from the literature, obtained using older interatomic potentials; namely, (i) data from Osetsky *et al.* (Ref. 21), obtained using the pair potential from Ref. 36, (ii) data from Marian *et al.* (Ref. 20), obtained using Ackland *et al.* (1997) potential (Ref. 42), and (iii) data from Soneda and de la Rubia (Ref. 19), obtained using the Johnson and Oh potential (Refs. 15, 59, and 63). Some data have been adequately treated in order to allow a consistent comparison (see text). The N^S law proposed by Osetsky *et al.* applies in all cases for the interpolation, with reasonable values for the S exponent.

It is known that, above a certain size, which certainly exceeds 100 SIA, the mobility of SIA clusters experiences a dramatic decrease.[21] However, the dynamic study of those clusters by MD becomes increasingly problematic because of the large size and the low mobility, so that the upper bound for the defects of class 3 is not clearcut and the issue of how to describe, in radiation damage accumulation models, the mobility of large and visible SIA clusters (dislocation loops) remains an open problem.

IV. DISCUSSION

A. Comparison with DFT results

We have seen that on two occasions, namely for the migration energy of the di- and tri-interstitial, the results dynamically obtained with the AMS potential do not agree with

static DFT calculations,[31,32] in spite of the proven capability of the EP to reproduce fairly well the properties of single SIA in accordance with DFT. In both cases, the discrepancy goes in the sense of lower migration energies in the dynamic calculations with EP. These discrepancies could, of course, be the consequence of a weakness of the EP. On the other hand, also DFT calculations have shortcomings that could question the full reliability of the obtained results. Dealing with SIA clusters, which have larger displacement fields than the single SIA, the use of small DFT boxes is likely to produce artefacts, caused by self-interaction of defects through periodic boundary conditions, and this may lead to an overestimation of the formation energy of the defect in its lowest energy state and to an even larger overestimation at the saddle point, thereby providing an overestimation of the migration energy. This could partly explain the higher migration energy found with DFT for the di- and tri-SIA clusters. The application of static procedures, on the other hand, restricts the study of transitions to predefined paths only and does not allow for vibrational entropy effects that become important at finite temperature.

B. Clusters of class 2: Features and problems

According to our findings the clusters of class 2, in contrast to defects of class 1, can take several different configurations during their migration, some of which allow them to glide along the close-packed ⟨111⟩ direction. As a result, an effectively faster mobility as compared to class 1 is observed, particularly in the low temperature regime (see Fig. 4). The smaller the $E_{\langle 111\rangle\text{-}\langle 110\rangle}$ difference of the given cluster, the easier the glide and therefore the closer its behavior to that of larger, purely 1D-migrating clusters. Note that these considerations will most likely remain true also using a potential capable of reproducing the relative stability of the single SIA exactly as predicted by DFT calculations,[31,32] since the key point is the relative stability of the whole cluster and not of the isolated SIA. The range of sizes of the SIA clusters belonging to class 2 might be different in this case; however, the existence of a "transition" class characterized by fairly complicated dynamic behavior during migration will most likely remain a matter of fact.

The complicated dynamic behavior of the clusters of this class requires, however, a careful treatment of the data and is not of easy interpretation. They were observed to glide fairly often, with a frequency of rotation from ⟨110⟩ to ⟨111⟩ that increases with cluster size. In particular, tetra- and penta-interstitial clusters spent a large part of MD time in the ⟨111⟩ configuration, which led to effective fast migration through glide, and this is consistent with the low static energy difference $E_{\langle 111\rangle\text{-}\langle 110\rangle}$. In the case of the tri-interstitial, however, $E_{\langle 111\rangle\text{-}\langle 110\rangle}$ is fairly large (larger than for di-interstitial); nonetheless, tri-interstitials were seen occasionally to reorient to the ⟨111⟩ configuration and glide, while di-interstitials were not. This may be explained taking into account that $E_{\langle 111\rangle\text{-}\langle 110\rangle}$ per SIA for the tri-interstitial is significantly smaller than for di-interstitial (see Table I), implying that the reorientation occurs in more than one step, involving one dumbbell at a time, rather than for the cluster as a whole, as confirmed by visual inspection. However, according to our analysis of the frequency of ⟨110⟩-to-⟨111⟩ reorientations, in the tri- and tetra-interstitial (Fig. 5) the involved activation energy is even lower than the $E_{\langle 111\rangle\text{-}\langle 110\rangle}$ energy difference per SIA, suggesting that the vibrational entropy contribution may be important in determining the stability of the cluster configuration at finite temperature. This is consistent with the enhanced 1D character of the migration of tri-interstitial at high temperature (above 600 K) and suggests that the vibrational entropies for ⟨110⟩ and ⟨111⟩ configurations must be different.

Finally, we have mentioned that the clusters of this class appear also to transform into anomalous and totally unexpected configurations, for which no simple migration mechanism can be devised, unless they first retransform into a regular configuration of parallel dumbbells or crowdions. The energy paths followed by these clusters during their migration at high temperature are thus complicated and hardly predictable by sole intuition. These frequent changes of configuration, which promote glide at high temperature and penalize it at low temperature, are likely to be the reason of the growth of f_c with temperature, in contrast to the behavior of f_c in the case of clusters of class 3.

Thus the complicated dynamic behavior of the clusters of this class poses problems related to the treatment to be applied for the assessment of their mobility. With an appropriate choice of τ_K and sufficiently long simulation times, ensuring a globally 3D motion, a diffusion coefficient can be estimated from MD simulations using the IIM and consequently an effective migration energy can be deduced from Eq. (2), with $n=3$, as has been done in the present work. However, this approach formally implies assigning at the atomic scale a fully 3D migration mechanism, which does not give its due to physics. On the other hand, the JLM cannot be used either if the studied defect involves a strong contribution from fully 3D migration, as was the case with tri-interstitial. Finally, the role and the effect on the effective cluster mobility of the anomalous configurations that appear occasionally is difficult to assess and may become apparent only beyond the MD timeframe.

C. Consequences in the prediction of radiation damage accumulation and annealing

The present study shows that the main consequences of a higher relative stability of the ⟨110⟩ dumbbell vs the ⟨111⟩ crowdion are in fact felt only in the case of small SIA clusters, while clusters formed by more than five SIAs behave in essentially the same way as predicted by earlier potentials. The latter statement may lead to hastily conclude that the differences found in this work are details of minor importance. In fact, this is not the case for at least two reasons.

First, it is well known from MD simulations that SIA clusters in α-Fe are produced already in displacement cascades,[15,22,24–29] at that most of these SIA clusters will be in the range of sizes where the difference between older and present potentials is significant, i.e., classes 1 and 2. The kinetics of the reactions between defects depends strongly on their dimensionality of motion: 1D migrating defects exhibit

smaller cross section of interaction with other defects than mixed 1D–3D migrating defects and these even smaller than fully 3D migrating defects.[1–4] Thus the short-term evolution of cascades, in particular the rate of recombination of SIA and SIA clusters with vacancies and vacancy clusters, as well as the rate of formation of larger SIA clusters, will necessarily be different in the case of rapidly 1D migrating clusters (old picture) than in the case of slower 3D or mixed 1D–3D migrating clusters (new picture).

Second, a detailed knowledge of the mobility of the single SIA and of small SIA clusters is essential for a correct interpretation of the low-temperature recovery stages, observed, e.g., in residual resistivity (RR) measurements[48,64] or magnetic after-effect (MAE) studies[65–70] of isochronally annealed α-Fe samples, after irradiation at very low temperature. According to standard nomenclature, the recovery takes place in five stages (a review and detailed bibliography, not only for iron—to which we shall exclusively refer here—can be found in Ref. 64). The standard interpretation assigns stages I and II to migration and subsequent annihilation of single SIAs and small SIA clusters at immobile vacancies or other sinks.[71,72] Stage I (20–150 K) exhibits a fine structure of low-temperature peaks associated to close pair recombination, correlated recombination (I_D) and free migration of the single SIA (I_E). Stage II (150–200 K) is generally resolved into one or two peaks, which are located at about 160 and 185 K, respectively,[48] and according to Ref. 48 are assigned to detrapping of single SIAs from C impurities and to free migration of the di-interstitial with an activation energy of 0.43 eV.[48,72] This value is coincident with the DFT-calculated one[31,32] suggesting that the discrepancy discussed in Sec. IV A should be settled in favor of the DFT value. However, in experimental works where the recovery has been monitored using positron annihilation spectroscopy,[73] the amount of single vacancies during stage II was observed to be constant, therefore the hypothesis of di-SIA recombination on vacancies fails. At the same time, the hypothesis of binding between the SIAs and C atoms contradicts DFT calculations suggesting repulsion rather than attraction.[74] Moreover, MAE studies reveal the appearance of recovery peaks *below* stage I_E in heating cycles that *follow* the annealing at temperatures *above* this stage.[65–70] These peaks grow at each re-annealing and re-cooling cycle and there is broad agreement between different researchers about at least three of them, located at about 50, 80, and 125 K, which always appear under neutron irradiation[65–67,70] and are weakly seen also after electron irradiation.[67,69,70] The associated activation energies have been deduced to be in the range of, respectively, 0.13–0.17 eV,[70] ~0.25 eV,[67] and 0.29–0.39 eV.[70] These activation energies have been associated with SIA clusters migrating faster than the single SIA, generally mentioning the di-interstitial as a candidate, or other more convoluted hypotheses.[45,65,69,70] Incidentally, the 50-K peak energies are similar to the migration energies found in this work for the tri- and tetra-interstitial, while the 125-K peak could correspond to the di-interstitial in the EP picture. Thus in itself the agreement of the DFT static calculation with the supposed migration energy of the di-interstitial according to *one of the possible interpretations* of RR studies is not sufficient to reject the quantitative results obtained in the present work, which may explain some of the observed MAE peaks. However, only careful studies with adequate models for these recovery stages, based on all the available information from atomic level investigations, can provide real indications to accept or refute the different existing interpretations of experimental data and, the other way around, to screen between acceptable and nonacceptable simulation results. In addition, the role of the anomalous configurations observed in this work on the actual mobility of SIA clusters beyond the MD time frame may also be nonnegligible and may participate in the interpretation of RR experiments.

V. CONCLUSIONS

A molecular-dynamics study of SIA and SIA cluster diffusion has been performed using an accurate empirical potential, that gives much higher relative stability to the ⟨110⟩ dumbbell vs the ⟨111⟩ crowdion than previous potentials for Fe, as suggested by DFT calculations. The results show that

(i) The applied EP predicts the dynamic migration energy of the single SIA to be about 0.3 eV, in agreement with experimental measurements, and the main mechanism of migration to be the one proposed by Johnson more than 40 years ago, in agreement with DFT calculations. It is the first time that a molecular dynamics study provides a migration energy for the single SIA essentially coincident with the experimental value.

(ii) Three classes of SIA defects can be distinguished, based not only on the dimensionality of their motion, but also on the physical migration mechanisms at the atomic level, namely,

(a) Class 1, composed by single and di-interstitial, characterised by fully 3D motion according to Johnson's mechanism.

(b) Class 2, composed by clusters formed by three to five SIAs, characterized by mixed 1D–3D motion and complex mechanisms of migration, that include the appearance of not only ⟨110⟩ and ⟨111⟩ configurations, but also anomalous ones. In these configurations the dumbbells are not parallel and migration is suppressed, very differently from the regular ones, that consist of parallel ⟨110⟩ dumbbells or ⟨111⟩ crowdions and clearly exhibit the possibility of migrating.

(c) Class 3, composed by all clusters formed by more than five SIAs, characterized by preferential 1D motion, by glide along ⟨111⟩ directions, with possible changes of ⟨111⟩ direction whose frequency, however, is out of reach for MD studies. Only the clusters of this class behave similarly to what was predicted also by earlier empirical potentials.

(iii) It is believed that these findings will change the results of simulations of the early stages of the microstructure evolution under irradiation, as well as the interpretation of recovery stages during annealing, as known from resistivity and magnetic measurements.

ACKNOWLEDGMENTS

The scientific advice of A. V. Barashev and Yu. N. Os-

etsky in the course of the realization of the present work is gratefully acknowledged. Thanks also to C. S. Becquart for reading the manuscript and suggesting useful corrections. This work was supported by the European Commission under the contract of Association between Euratom and the Belgian State and carried out within the framework of the European Fusion Development Agreement (EFDA), Task No. TTMS-007.

*Corresponding author. FAX: +32-14-321216. Email address: dterenty@sckcen.be

[1] H. Trinkaus, B. N. Singh, and A. J. E. Foreman, J. Nucl. Mater. **199**, 5 (1992); **206**, 200 (1993); **251**, 172 (1997).
[2] H. Trinkaus, B. N. Singh, and S. I. Golubov, J. Nucl. Mater. **283-287**, 89 (2000).
[3] H. L. Heinisch, B. N. Singh, and S. I. Golubov, J. Nucl. Mater. **276**, 59 (2000); **283-287**, 737 (2000).
[4] H. L. Heinisch and B. N. Singh, Philos. Mag. **83**, 3661 (2003).
[5] B. N. Singh, S. I. Golubov, H. Trinkaus, A. Serra, Yu. N. Osetsky, and A. V. Barashev, J. Nucl. Mater. **251**, 107 (1997).
[6] S. I. Golubov, B. N. Singh, and H. Trinkaus, J. Nucl. Mater. **276**, 78 (2000).
[7] M. J. Caturla, N. Soneda, E. Alonso, B. D. Wirth, T. Díaz de la Rubia, and J. M. Perlado, J. Nucl. Mater. **276**, 13 (2000).
[8] N. Soneda, S. Ishino, A. Takahashi, and K. Dohi, J. Nucl. Mater. **323**, 169 (2003).
[9] C. Domain, C. S. Becquart, and L. Malerba, J. Nucl. Mater. **335**, 121 (2004).
[10] R. Bullough and R. C. Perrin, Proc. R. Soc. London, Ser. A **305**, 541 (1968).
[11] J. M. Harder and D. J. Bacon, Philos. Mag. **58**, 165 (1988).
[12] B. D. Wirth, G. R. Odette, D. Maroudas, and G. E. Lucas, J. Nucl. Mater. **244**, 185 (1997).
[13] Yu. N. Osetsky, M. Victoria, A. Serra, S. I. Golubov, and V. Priego, J. Nucl. Mater. **251**, 34 (1997).
[14] Yu. N. Osetsky, A. Serra, and V. Priego, in *Diffusion Mechanisms in Crystalline Materials*, edited by Y. Mishin, G. Vogl, N. Cowen, and R. Callow, Mater. Res. Soc. Symp. Proc. (Materials Research Society, Pittsburgh, 1998), p. 59.
[15] N. Soneda and T. Díaz de la Rubia, Philos. Mag. A **78**, 995 (1998).
[16] Yu. N. Osestky, D. J. Bacon, A. Serra, B. N. Singh, and S. I. Golubov, J. Nucl. Mater. **276**, 65 (2000).
[17] Yu. N. Osestky, A. Serra, B. N. Singh, and S. I. Golubov, Philos. Mag. A **80**, 2131 (2000).
[18] B. D. Wirth, G. R. Odette, D. Maroudas, and G. E. Lucas, J. Nucl. Mater. **276**, 33 (2000).
[19] N. Soneda and T. Díaz de la Rubia, Philos. Mag. A **81**, 331 (2001).
[20] J. Marian, B. D. Wirth, A. Caro, B. Sadigh, G. R. Odette, J. M. Perlado, and T. Díaz de la Rubia, Phys. Rev. B **65**, 144102 (2002).
[21] Yu. N. Osetsky, D. J. Bacon, A. Serra, B. N. Singh, and S. I. Golubov, Philos. Mag. **83**, 61 (2003).
[22] C. S. Becquart, C. Domain, A. Legris, and J-C. Van Duysen, J. Nucl. Mater. **280**, 73 (2000).
[23] L. Malerba, J. Nucl. Mater. **351**, 28 (2006).
[24] A. F. Calder and D. J. Bacon, J. Nucl. Mater. **207**, 25 (1993).
[25] W. J. Phytian, A. J. E. Foreman, R. E. Stoller, D. J. Bacon, and A. F. Calder, J. Nucl. Mater. **223**, 245 (1995).
[26] R. E. Stoller, G. R. Odette, and B. D. Wirth, J. Nucl. Mater. **251**, 49 (1997).
[27] R. E. Stoller, J. Nucl. Mater. **276**, 22 (2000).
[28] D. A. Terentyev, L. Malerba, and M. Hou, Nucl. Instrum. Methods Phys. Res. B **228**, 156 (2005).
[29] D. A. Terentyev, C. Lagerstedt, P. Olsson, K. Nordlund, J. Wallenius, and L. Malerba, J. Nucl. Mater. **351**, 65 (2006).
[30] C. Domain and C. S. Becquart, Phys. Rev. B **65**, 024103 (2001).
[31] Chu-Chun Fu, F. Willaime, and P. Ordejón, Phys. Rev. Lett. **92**, 175503 (2004).
[32] F. Willaime, C. C. Fu, M. C. Marinica, and J. Dalla Torre, Nucl. Instrum. Methods Phys. Res. B **228**, 92 (2005).
[33] V. Hivert, R. Pichon, H. Bilger, P. Bichon, J. Verdone, D. Dautreppe, and P. Moser, J. Phys. Chem. Solids **31**, 1843 (1970).
[34] W. Chambron, J. Verdone, and P. Moser, in *Fundamental Aspects of Radiation Damage in Metals*, edited by M. T. Robinson and F. W. Young, Jr., ERDA Report, Conf. 751006 NT 15, Springfield, VA, 1976, p. 261.
[35] P. Ehrhart, K. H. Robrocka, and H. R. Schober, in *Physics of Radiation Effects in Crystals*, edited by R. A. Johnson and A. N. Orlov (Elsevier, Amsterdam, 1986), p. 7, and references therein.
[36] Yu. N. Osetsky, A. G. Mishin, and A. Serra, Philos. Mag. A **72**, 361 (1995).
[37] G. Simonelli, R. Pasianot, and E. J. Savino, in *Materials Theory and Modelling*, edited by J. Broughton, P. D. Bristowe, and J. M. Newsam, Mater. Res. Soc. Symp. Proc. (Materials Research Society, Pittsburgh, 1993), p. 567.
[38] D. A. Terentyev, L. Malerba, R. Chakarova, K. Nordlund, P. Olsson, M. Rieth, and J. Wallenius, J. Nucl. Mater. **349**, 119 (2006).
[39] R. A. Johnson, Phys. Rev. **134**, A1329 (1964).
[40] J. M. Harder and D. J. Bacon, Philos. Mag. A **54**, 651 (1986).
[41] G. Simonelli, R. Pasianot, and E. J. Savino, Phys. Status Solidi B **191**, 249 (1995).
[42] G. J. Ackland, D. J. Bacon, A. Calder, and T. Harry, Philos. Mag. A **75**, 713 (1997).
[43] G. Simonelli, R. C. Pasianot, and E. J. Savino, Phys. Status Solidi B **217**, 747 (2000).
[44] F. Gao, D. J. Bacon, A. V. Barashev, and H. L. Heinisch, in *Microstructural Processes in Irradiated Materials*, edited by S. J. Zinkle, G. E. Lucas, R. C. Ewing, and J. S. Williams, Mater. Res. Soc. Symp. Proc. (MRS, Warrendale, PA, 1999), p. 703.
[45] H. Bilger, V. Hivert, J. Verdone, J. L. Leveque, and J. C. Soulis, in *Proceedings of the International Conference on Vacancies and Insterstitials in Metals*, Jül-Conf-2 Vol. II, Sept. 23–28, KFA Jülich, Germany, 1968, p. 751.
[46] J. Verdone, W. Chambron, and P. Moser, Phys. Status Solidi B **61**, K41 (1974).
[47] H.-E. Schaefer, D. Buttweg, and W. Dander, in *Proceedings of the International Conference on Fundamental Aspects of Radiation Damage in Metals*, edited by M. T. Robinson and F. W. Young, ERDA Report, Conf. 751006 NT 15, Springfield, Virginia, 1976,

Vol. I, p. 463.
[48] S. Takaki, J. Fuss, H. Kugler, U. Dedek, and H. Schultz, Radiat. Eff. **79**, 87 (1983).
[49] M. I. Mendelev, S. Han, D. J. Srolovitz, G. J. Ackland, D. Y. Sun, and M. Asta, Philos. Mag. **83**, 3977 (2003).
[50] G. J. Ackland, M. I. Mendelev, D. J. Srolovitz, S. Han, and A. V. Barashev, J. Phys.: Condens. Matter **16**, 1 (2004).
[51] Yu. N. Osetsky, Defect Diffus. Forum **188-190**, 71 (2001).
[52] P. G. Shewmon, *Diffusion in Solids* (McGraw-Hill, New York, 1963), p. 52.
[53] M. W. Guinan, R. N. Stuart, and R. J. Borg, Phys. Rev. B **15**, 699 (1977).
[54] J. R. Manning, *Diffusion Kinetics for Atoms in Crystals* (Van Nostrand, London, 1968), p. 88.
[55] Yu. N. Osetsky and A. Serra, Defect Diffus. Forum **143-147**, 155 (1997).
[56] R. C. Pasianot, A. M. Monti, G. Simonelli, and E. J. Savino, J. Nucl. Mater. **276**, 230 (2000).
[57] D. Terentyev and L. Malerba, J. Nucl. Mater. **329-333**, 1161 (2004).
[58] S. M. J. Gordon, S. D. Kenny, and R. Smith, Phys. Rev. B **72**, 214104 (2005).
[59] M. Guellil and J. B. Adams, J. Mater. Res. **7**, 639 (1992).
[60] R. Chakarova, V. Pontikis, and J. Wallenius, Delivery Report WP6, SPIRE project, EC Contract No. FIKW-CT-2000-00058, June 2002, available at www.neutron.kth.se/publications/library/DR-6.pdf
[61] A. V. Barashev, Yu. N. Osetsky, and D. J. Bacon, Philos. Mag. A **80**, 2709 (2000).
[62] A. V. Barashev, Yu. N. Osetsky, and D. J. Bacon, in *Microstructural Processes in Irradiated Materials*, edited by S. J. Zinkle, G. E. Lucas, R. C. Ewing, and J. S. Williams, Mater. Res. Soc. Symp. Proc. Materials Research Society, Warrendale, PA, 1999, p. 697.
[63] R. A. Johnson and D. J. Oh, J. Mater. Res. **4**, 1195 (1989).
[64] *Atomic Defects in Metals*, edited by Landolt-Börnstein, New Series, Group III, Vol. 25 (Spinger-Verlag, Berlin, 1991).
[65] E. Balthesen, K. Isebeck, and H. Wenzl, Phys. Status Solidi **8**, 603 (1965).
[66] P. Moser, Mem. Sci. Rev. Metall. **63**, 431 (1966).
[67] F. Walz, H. Schreyer, and H. Kronmüller, Phys. Status Solidi A **43**, K81 (1977).
[68] W. Mensch and J. Diehl, Phys. Status Solidi A **43**, K175 (1977).
[69] J. Verdone, P. Moser, W. Chambron, J. Johansson, P. Hautojärvi, and A. Vehanen, J. Magn. Magn. Mater. **19**, 296 (1980).
[70] H. J. Blythe, H. Kronmüller, A. Seeger, and F. Walz, Phys. Status Solidi A **181**, 233 (2000).
[71] We shall not consider here the so-called two-interstitial model, that assigns also stage III to the migration of an interstitial species (Ref. 70), because such interpretation is not consistent with the DFT description of the single SIA (and of the vacancy) in α-Fe, which lies at the basis of the present work.
[72] C.-C. Fu, J. Dalla Torre, F. Willaime, J. L. Bocquet, and A. Barbu, Nat. Mater. **4**, 68 (2005).
[73] A. Vehanen, P. Hautojärvi, J. Johansson, J. Yli-Kauppila, and P. Moser, Phys. Rev. B **25**, 762 (1982).
[74] C. Domain, C. S. Becquart, and J. Foct, Phys. Rev. B **69**, 144112 (2004).
[75] P. Olsson, L. Malerba, and A. Almazouzi, SCK-CEN Report BLG-950, June 2003.